OPTICAL REVIEW Vol. 21, No. 5 (2014) 668–675

Dual Focus Diffractive Optical Element with Extended Depth of Focus

Katsuhiro UNO[1]* and Isao SHIMIZU[2]

[1]*Graduate School of Science and Engineering, Faculty of Engineering, Ibaraki University, Hitachi, Ibaraki 316-8511, Japan*
[2]*Research Institute of Advanced Technology (RIAT), Naka, Ibaraki 319-2103, Japan*

(Received March 31, 2014; Revised May 23, 2014; Accepted June 13, 2014)

A dual focus property and an extended depth of focus were verified by a new type of diffractive lens displaying on liquid crystal on silicon (LCoS) devices. This type of lens is useful to read information on multilayer optical discs and tilted discs. The radial undulation of the phase groove on the diffractive lens gave the dual focus nature. The focal extension was performed by combining the dual focus lens with the axilens that was invented for expanding the depth of focus. The number of undulations did not affect the intensity along the optical axis but the central spot of the diffraction pattern.

Keywords: dual focus lens, extended depth of focus, axilens, daisy lens, lotus lens

1. Introduction

Recently, the optical pickup system has met problems related to disc compatibility. How do you read DVDs and CDs using one pickup lens? How do you read double layers on a DVD simultaneously? We must overcome the focusing error due to the different thicknesses of the substrate and layers. A simple method now widely used is to move the focal spot of the lens mechanically by a complicated servo system. Another remedy for these problems is a dual focusing system. Some researchers have developed several methods of dual focusing. The twin rotating lens system is used to mechanically switch optimal lenses for CDs and DVDs.[1)] A holographic lens was inserted into the focusing lens, which produced twin beams with different focal lengths by zero- and +1st-order diffracted light waves.[2)] A liquid crystal shutter was used for controlling the numerical aperture (NA) of the condenser lens by varying the aperture diameter by polarization control.[3)] An annular mask was attached on the objective lens to separate near-axis rays from outer-peripheral rays, which have different focal points.[4)]

Another focusing error comes from disc misalignment due to disc vibration and tilt. What kind of pickup system is tolerant of disc tilt and wobble? A focus tracking system by servo motors is also available. However, it is difficult to catch up with such rapid focal variation. Another method compensating for this problem is to elongate the focal length of the lens. The axilens is one of the suitable candidates for extending the focal depth, which was invented by combining an axicon with a spherical lens.[5)] The axicon is a device that converts a plane wave into a Bessel beam (non-diffracting beam).[6)]

We have been using a spatial light modulator such as a liquid crystal on silicon (LCoS) display as a light-concentrating device. We have succeeded in converting the plane wave into the spherical wave by reflecting the incoming beam on the LCoS display that depicts a gray-scale image corresponding to the phase distribution such as a Fresnel lens. We have also changed the focal length of the lens only by changing the displaying image. Such a lens-less system will bring more compact and flexible systems. The purpose of this study is to find a diffractive lens with dual focus and a large focal depth, which is available for spatial light modulators. Numerical simulation of light propagation diffracted by the diffractive lens displayed on the spatial light modulator was performed in this study.

In Sect. 2, we mathematically define the phase profiles of the diffractive lens. As well as the conventional Fresnel lens and the axilens,[5)] we also define new types of lens profiles named the daisy lens, dual-focus lens, and lotus lens. We adopted scalar diffraction theory to calculate intensity profiles diffracted from diffractive lenses with only a low F-number. The diffraction integral that we used in the simulation and the angular spectrum method for the fast calculation of diffraction patterns are also explained briefly in this section. In Sect. 3, the phase profiles of the diffractive lens that we used in the simulation are shown. For simplicity, the phase function that we considered in the simulation has a continuous phase level modulo 2π and has no wavelength mismatch, which leads to a diffraction efficiency of 100% for the designed wavelength.[7,8)] The results of axial intensity profiles and lateral intensity profiles (diffraction patterns) are also shown in this section. Some concluding remarks are provided in Sect. 4.

2. Theory

2.1 *Phase function of diffractive lens*

A paraxial approximation of a spherical lens, which converts an incoming monochromatic plane wave into a spherical wave, has a transmission function expressed as

$$t(r) = \exp[-i\pi\phi(r)], \tag{1}$$

$$\phi(r) = \frac{r^2}{\lambda f}, \tag{2}$$

where $r = (x^2 + y^2)^{1/2}$ is the radial coordinate, f is the focal length of the holographic lens, and λ is the wavelength. To convert the conventional spherical lens to the diffractive Fresnel lens, the maximum phase modulation is $2m\pi$,

*E-mail address: k-uno@mx.ibaraki.ac.jp

$(m = 1, 2, \ldots)$.[8] Then, the phase function of the Fresnel lens can be rewritten as[7]

$$\psi(r) = 2\pi\alpha\left[m - \left(\frac{1}{2}\phi(r) \bmod m\lambda\right)\right], \tag{3}$$

where α is the fraction of the 2π phase delay that is introduced for wavelength mismatch and $\phi(r)$ is the same as Eq. (2). The function, A mod B, returns a residue of A divided by B.

There is an axilens as one of the long focal depth lenses. The phase function of the axilens on the right-hand side of Eq. (3) is written as[5]

$$\phi(r) = \frac{r^2}{\lambda\left(f_0 + \dfrac{\delta z}{R^2}r^2\right)}, \tag{4}$$

where f_0 is the initial focal length, R is the radius of the lens, and δz is the focal depth. The geometrical optics predicts that the axilens has a continuous focal line in the range of $f_0 < z < f_0 + \delta z$. The focal length of the axilens is $f_0 + (\delta z/R^2)r^2$ and is a function of radial coordinate r. This means that the axilens consists of a continuously distributed annular spherical lens with different focal lengths.

On the other hand, the dual focus lens is composed of several azimuthally varying spherical lenses. Sinusoidal variation along the azimuthal angle of the lens, which is called a daisy lens elsewhere, was invented to produce a dual focus beam with an extended depth of focus.[9] The phase function of the daisy lens is written as

$$\phi(r) = \frac{r^2}{\lambda f_0[1 + b\sin(n\theta)]}, \tag{5}$$

where b means the modulation depth of azimuthal undulation and n means the number of daisy petals. The focal length of the daisy lens is considered to be continuously distributed from $f_0(1 - b)$ to $f_0(1 + b)$. We deduce that more energy is distributed at the focal lengths where the stationary points of sinusoidal function are. Accordingly, the daisy lens is thought to have dual focus.

We newly created an other type of dual focus lenses expressed by

$$\phi(r) = \frac{r^2}{\lambda f_0(1 + b\{\mathrm{sgn}[\sin(n\theta)]\})}, \tag{6}$$

where $\mathrm{sgn}(x)$ is the signature function defined as

$$\mathrm{sgn}(x) = \begin{cases} 1 & x \geq 0 \\ 0 & x < 0 \end{cases}.$$

The dual-focus lens that we named has a square-wave variation of focal length along the azimuthal angle. This means that the focal length of the dual-focus lens has only two values of $f_0(1 - b)$ and $f_0(1 + b)$.

We also developed other new types of the holographic lens, which were created by combining the dual-focus lens with an axilens. We intended that these combined dual focus lenses have a long focal line around the two main focal points. The axi-daisy lens was composed of a daisy lens and an axilens, which may have the focal ranges of $f_0(1 - b) < z < f_0(1 - b) + \delta z$ and $f_0(1 + b) < z < f_0(1 + b) + \delta z$. The axi-daisy lens has a phase profile defined as

$$\phi(r) = \frac{r^2}{\lambda\left\{f_0[1 + b\sin(n\theta)] + \dfrac{\delta z}{R^2}r^2\right\}}. \tag{7}$$

The dual-focus axilens was a combined version of the dual-focus lens and axilens, which may have the same focal range as the axi-daisy lens. The phase function of the dual-focus axilens is defined as

$$\phi(r) = \frac{r^2}{\lambda\left\{f_0(1 + b\{\mathrm{sgn}[\sin(n\theta)]\}) + \dfrac{\delta z}{R^2}r^2\right\}}. \tag{8}$$

The lotus lens is different from the previous two types of lenses. The focal variation of the lotus lens is an azimuthal triangular-wave form, which is defined as

$$\phi(r) = \frac{r^2}{\lambda f_0\left\{1 + b\left[\left|\dfrac{4n\theta}{2\pi}\right| - \left(\dfrac{n\theta}{2\pi}\right)\right]\right\}}. \tag{9}$$

The focal range of the lotus lens may be the same as that of the daisy lens. However, the amount of energy distributed to each focal length is equal in the focal range on account of the linear wave form. Therefore, the intensity of the focal spot may be more uniform along the focal range than the daisy lens. The lotus axilens is a combined version of the lotus lens and an axilens. The phase function of the lotus axilens is defined as

$$\phi(r) = \frac{r^2}{\lambda\left\{f_0\left(1 + b\left[\left|\dfrac{4n\theta}{2\pi}\right| - \left(\dfrac{n\theta}{2\pi}\right)\right]\right) + \dfrac{\delta z}{R^2}r^2\right\}}. \tag{10}$$

2.2 *Wave propagation theory for simulation*

We performed computer simulation of the diffraction field of the holographic lens. We calculated the intensity profile around the optical axis and lateral profiles (diffraction patterns) at several propagation distances z. A scalar diffraction theory was used in the simulation, because we consider a relatively low NA situation. The Huygens–Fresnel diffraction integral defined as[10]

$$U(r, z) = \iint_{\Sigma} A(r)\exp\left(\frac{iks}{s}\right)(1 + \cos\chi)\, dS, \tag{11}$$

was used in the calculation, where Σ represents the area inside the pupil, $r = (x^2 + y^2)^{1/2}$, and $s = (r^2 + z^2)^{1/2}$. χ means the angle between a vector along the optical axis and a vector along the line s. We used this integral for calculation of the intensity profile around the optical axis after data discretization.

Additionally, we calculated diffraction patterns at several propagation distances z. Instead of using Eq. (11), the calculation of the diffraction pattern was performed by the shifted-angular spectrum method, which was invented by Matsushima,[11] to save calculation time. The shifted-angular spectrum method is explained as follows. Considering the situation where the object wave $g(x, y, 0)$ leads to $\hat{g}(x, y, z_0)$

after the propagation z_0 (> 0), the calculation procedure is as follows:

$$\hat{g}(\hat{x}, \hat{y}, z_0) = F^{-1}[\hat{G}(u, v; z_0)], \tag{12}$$

$$\hat{G}(u, v; z_0) = G(u, v, 0)\hat{H}(u, v; z_0), \tag{13}$$

$$G(u, v, 0) = F[g(x, y, 0)], \tag{14}$$

$$\hat{H}(u, v, z_0) = \exp[i2\pi(x_0 u + y_0 v + z_0 w)], \tag{15}$$

$$w = w(u, v) = \begin{cases} (\lambda^{-2} - u^2 - v^2)^{1/2} \\ \qquad u^2 + v^2 \le \lambda^{-2} \\ 0 \qquad \text{otherwize} \end{cases}. \tag{16}$$

Here, $F[\cdot]$ and $F^{-1}[\cdot]$ represent the Fourier transform and its inverse transform, respectively. x_0 and y_0 are the coordinate shifts between the object plane (x, y) and the propagated plane $(\hat{x}, \hat{y})$, respectively. Actually, the transfer function $\hat{H}$ of the point spread function is band-limited to suppress aliasing noise as follows:

$$\hat{H}'(u, v; z_0) = \hat{H}(u, v; z_0)\,\mathrm{rect}\left(\frac{u - u_0}{u_w}\right)\mathrm{rect}\left(\frac{v - v_0}{v_w}\right). \tag{17}$$

Here, the rect(x) function is defined as

$$\mathrm{rect}(x) = \begin{cases} 1 & |x| \le 1/2 \\ 0 & |x| > 1/2 \end{cases},$$

and u_0 and u_w are defined as[11]

$$u_0 = \begin{cases} \dfrac{u_l^{(+)} + u_l^{(-)}}{2} & S_x < x_0 \\ \dfrac{u_l^{(+)} - u_l^{(-)}}{2} & -S_x \le x_0 < S_x, \\ \dfrac{-(u_l^{(+)} + u_l^{(-)})}{2} & x_0 \le -S_x \end{cases} \tag{18}$$

$$u_w = \begin{cases} u_l^{(+)} - u_l^{(-)} & S_x < x_0 \\ u_l^{(+)} + u_l^{(-)} & -S_x \le x_0 < S_x, \\ u_l^{(-)} - u_l^{(+)} & x_0 \le -S_x \end{cases} \tag{19}$$

where S_x represents the maximum size of the object plane and $u_l^{(\pm)}$ is written as

$$u_l^{(\pm)} = [(x_0 \pm S_x)^{-2} z_0^2 + 1]^{-1/2} \lambda^{-1}. \tag{20}$$

The same notation is applied to v_0 and v_w.

3. Results and Discussion

3.1 Phase profile of the diffractive lens

The holographic diffractive lenses defined in the previous section are shown in Fig. 1. The initial focal length was set to $f_0 = 200$ mm for all diffractive lenses. Other parameters of each lens are described in the figure caption. The case of the normal Fresnel lens is shown in Fig. 1(a) for comparison. The focal depth δz of the axilens, axi-daisy lens, dual-focus axilens, and lotus axilens was set to 20 mm. The modulation depth b of the daisy lens, axi-daisy lens, dual-focus lens, dual-focus axilens, lotus lens, and lotus axilens was set to 0.1, which means that the focal point shifts by 10% from the initial focal length. We set the diameter of the diffractive lens to about 8 mm.

The daisy lens is similar to the axi-daisy lens. The dual-focus lens and the dual-focus axilens are also similar. Slight differences in lateral phase retardation between the Fresnel lens and the axilens are shown in Fig. 2. The axilens has larger blaze pitch than that of the Fresnel lens at larger radius. Other types of diffractive lens pairs have a similar trend.

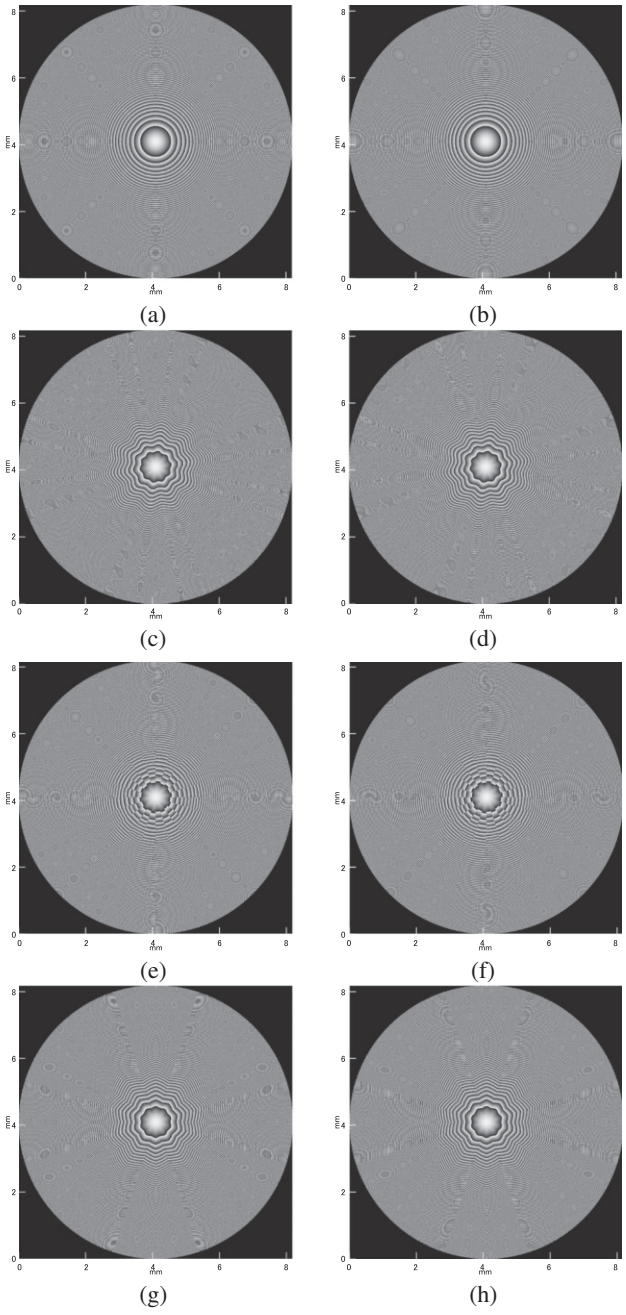

Fig. 1. Phase profile of diffractive lens with $f_0 = 200$ mm. (a) Fresnel lens. (b) Axilens with $\delta z = 20$ mm. (c) Daisy lens with $b = 0.1$ and $n = 10$. (d) Axi-daisy lens with $\delta z = 20$ mm, $b = 0.1$, and $n = 10$. (e) Dual-focus lens with the same parameters as (c). (f) Dual-focus axilens with the same parameters as (d). (g) Lotus lens with the same parameters as (c). (h) Lotus axilens with the same parameters as (c).

3.2 Intensity distribution around the optical axis

The intensity profiles around the optical axis of these

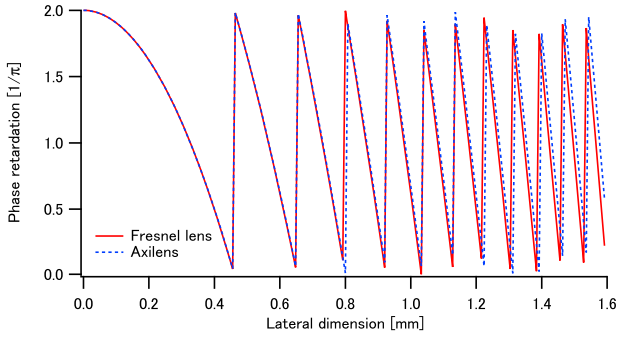

Fig. 2. (Color online) Lateral phase retardation profiles of Fresnel lens and axilens.

diffractive lenses are shown in Fig. 3. In these figures, the lateral radius of the vertical axis is 0.1 mm and the axial distance is from 0.16 to 0.25 m, except for Fig. 3(f). As we expected, the Fresnel lens has a single focal spot at $z = 0.2$ m. Twin peaks of the intensity profile appear in the daisy lens, dual-focus lens, and lotus lens. The positions of the intensity peaks are 0.18 and 0.22 m, which are equal to $f_0(1 - b)$ and $f_0(1 + b)$, respectively, as predicted in Sect. 2. The intensity ratio of the two peaks against the intensity values around these peaks in the dual-focus lens case, as shown in Fig. 3(e), is stronger than that in other dual focus diffractive lens cases, i.e., the daisy lens [Fig. 3(c)] and lotus lens [Fig. 3(g)], which means that more energy concentrates at the two focal points. The lotus lens has more blurred intensity peaks than the others. The reason why two peaks are blurred is explained later. The axilens has a long focal depth behind the initial focal length, as shown in Fig. 3(b). However, the intensity profile along the optical axis is not uniform. This may be the result of an interference effect of the adjacent focal depth. Some fringe in the intensity distribution around the optical axis appears to reflect this effect. The axi-daisy lens, dual-focus axilens, and lotus axilens have two focal peaks with relatively long focal depths. The uniformity of these peaks is not so good because of the interference effect. The focal depths of the two peaks in the axi-daisy lens [Fig. 3(d)], and lotus axilens [Fig. 3(h)] are shorter than those of the dual-focus axilens [Fig. 3(f)]. This may come from the waveform of undulation of the lens profile. Sine curve undulation in the axi-daisy lens and the triangular form in the lotus lens bring the interference effect on the diffraction pattern not only in the radial direction but also in the azimuthal direction. On the other hand, the dual-focus axilens has only two state variation, so that the interference does not arise in the azimuthal direction. The lotus axilens has a semi-periodic variation of intensity distribution. This may come from the equipartition of energy along the optical axis emanated from the triangular wave form of phase groove undulation.

Axial intensity distributions of diffraction patterns of the diffractive lenses are shown in Fig. 4. The relative intensity scaling of Fig. 4(a) is the same as that of Figs. 4(b) and 4(c), so that we can compare the values of those intensity profiles with each other. The Fresnel lens, dual-focus lens, and axilens belong to the relatively high intensity profile group. The daisy lens and dual-focus axilens are in the middle class of peak intensity. The axi-daisy lens, lotus lens, and lotus axilens have only comparatively low intensity profiles. The dual-focus lens and daisy lens have two sharp intensity peaks at the same focal lengths. However, the relative intensity of the dual-focus lens is about 20 times greater than that of the daisy lens, which is about 4 times larger than that of the lotus lens. Continuous focal variation of the daisy lens distributes the light energy around the focal line, while the binarized focal variation of the dual-focus lens concentrates the energy only on the two focal points. We think that this is the reason for the result. The lotus lens also has two intensity peaks at around the same position of the daisy lens. However, the intermediate focal lengths between the two peaks also have relatively high intensity values. We attribute those high intensity values to the rays that emanate from the linearly oscillated zone undulation of the lotus lens and arrive at equally spaced focal points. The lotus lens seems to have a focal expansion effect without combination with an axilens.

The axilens and the dual-focus axilens have broad intensity profiles, which are shifted to longer focal lengths. The width between two ends of the peaks, which are indicated by arrows, of the axilens was about 0.02 m, which is equal to the focal depth δz. The dual-focus axilens has the broadest profile, the length of which is almost twice that of the axilens. We understand that the two intensity peaks elongated their focal depths and connected each other. The twin peaks of the axi-daisy lens were broader than those of the daisy lens, while the width of each peak was smaller than the predicted value of δz. In the intermediate focal length between two peaks, the intensity value appears to be oscillating. This may be a consequence of the interference between two broad peaks. The lotus axilens is similar to the axi-daisy lens.

Normalized lateral intensity profiles of each lens are shown in Fig. 5. Each focal distance where we measured the lateral intensity is written in the legend of the figure. The lateral intensity profiles were measured at the most prominent part of the profile in Fig. 3. Therefore, we assure that the main lobe width of all types of lens is not more than that in Fig. 5. We collected the results of the long-focus-type lens in Fig. 5(a) and the results of the dual-focus-type lens in Fig. 5(b). In Fig. 5(a), the main lobe widths of the axilens, axi-daisy lens, dual-focus axilens, and lotus axilens are greater than that of the Fresnel lens. The half width at half maximum of the dual-focus axilens at $z = 0.188$ m, the narrowest case, is about 1.4 times bigger than that of the Fresnel lens. The intensity curve at $z = 0.231$ m, another prominent point, was almost the same as $z = 0.188$ m. The same tendency was also seen in the axi-daisy lens case. It is worth noting that the main lobe width of the dual-focus axilens is smaller than that of the axilens.

In Fig. 5(b), the main lobe width of the dual-focus lens at $z = 0.18$ m is slightly smaller than the Fresnel lens case, while a bigger lobe width is seen in the case of $z = 0.22$ m, which is another focal point. The daisy lens at $z = 0.18$ m also has a sharp intensity peak comparable to the Fresnel

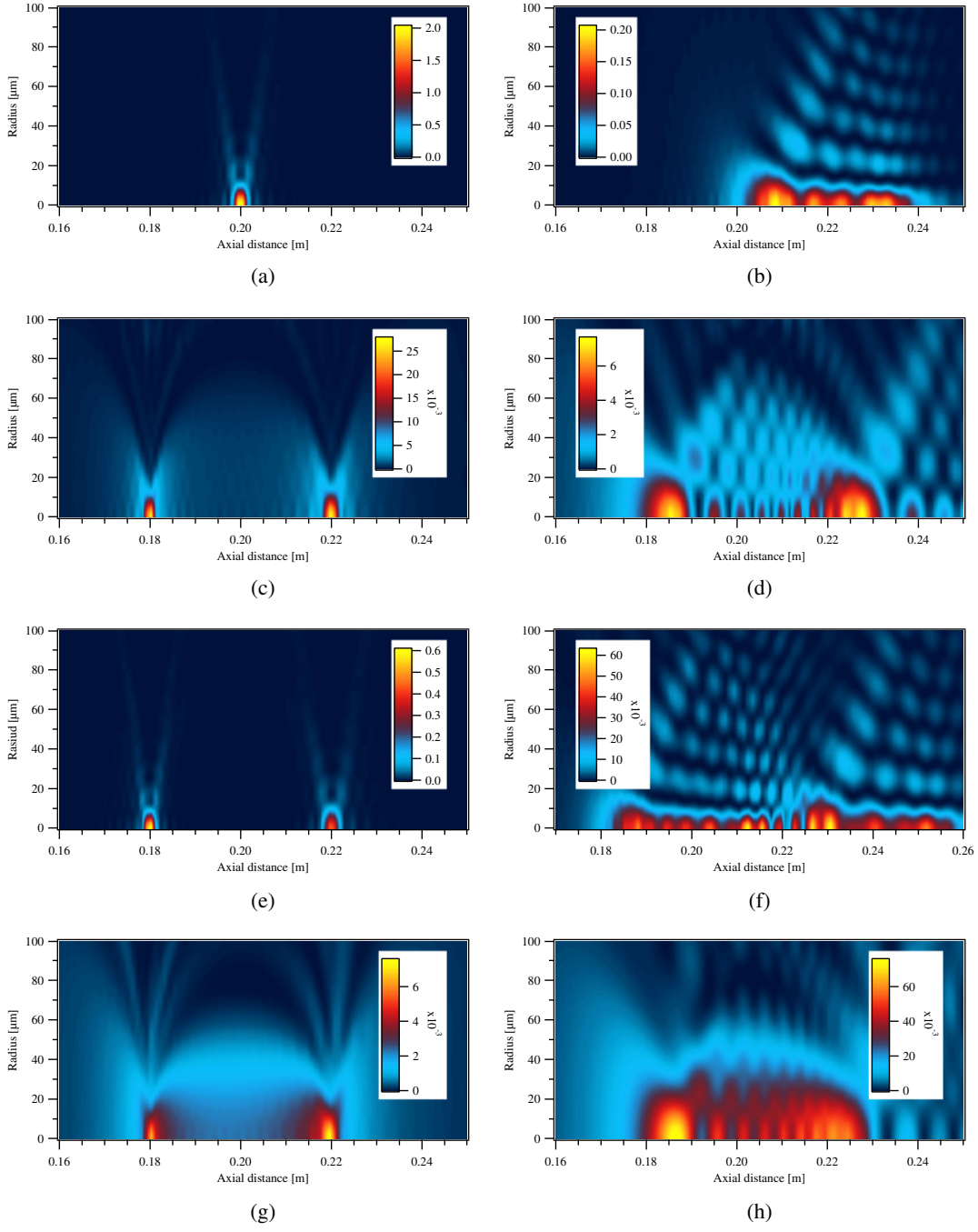

Fig. 3. (Color online) Intensity distributions around the optical axis of diffractive lens with $f_0 = 200$ mm. (a) Fresnel lens. (b) Axilens with $\delta z = 20$ mm. (c) Daisy lens with $b = 0.1$ and $n = 10$. (d) Axi-daisy lens with $\delta z = 20$ mm, $b = 0.1$, and $n = 10$. (e) Dual-focus lens with the same parameters as (c). (f) Dual-focus axilens with the same parameters as (d). (g) Lotus lens with the same parameters as (c). (h) Lotus axilens with the same parameters as (d).

lens case. The lotus lens cases have broader lobes than the others. We found that the longer focal points have broader lobes than the shorter focal points, as shown in the figure. This is a natural consequence of the focal spot being proportional to the focal length, which is deduced from the Airy pattern.[12)]

3.3 *Diffraction patterns*

Diffraction patterns of the holographic lens at several focal distances are shown in Fig. 6. The measurement points of all figures are the same as in Fig. 5. The spot size of the beams at the shorter focal points in the dual focus case will be smaller than that in Fig. 6. The Fresnel lens appears to have the smallest spot size of $d \simeq 16\,\mu$m. However, the dual-focus lens also has a small spot comparable to the Fresnel lens. Other lenses have bigger spots than those two cases. These findings are supported by the results in Fig. 5.

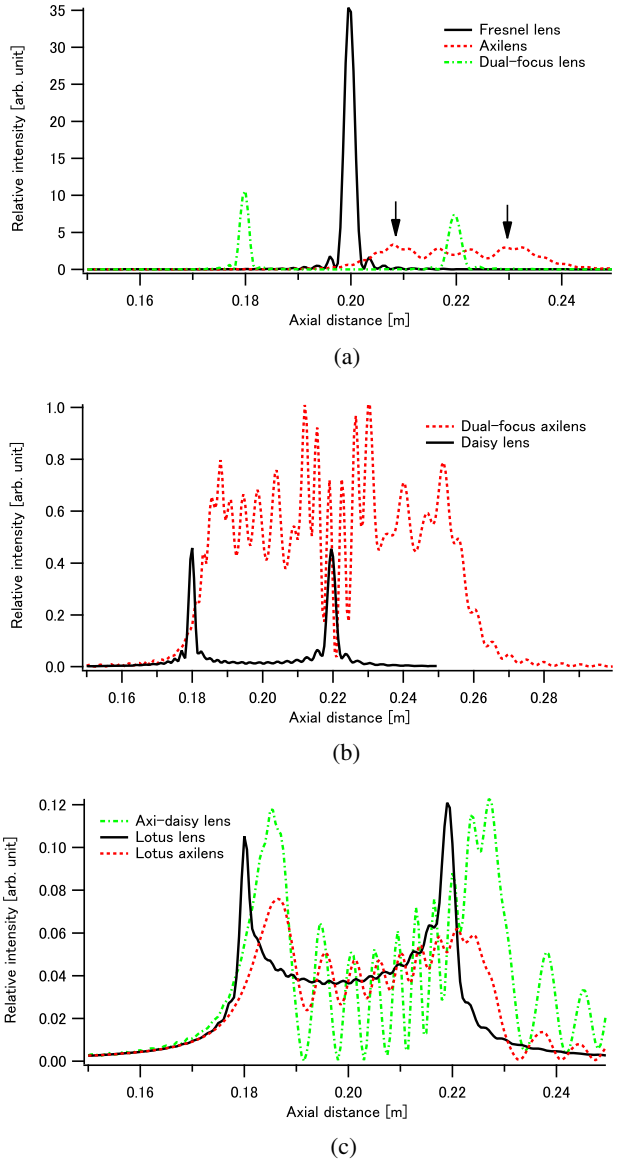

Fig. 4. (Color online) Intensity profile on the optical axis. (a) Fresnel lens, axilens, and dual-focus lens. (b) Daisy lens and dual-focus axilens. (c) Axi-daisy lens, lotus lens, and lotus axilens.

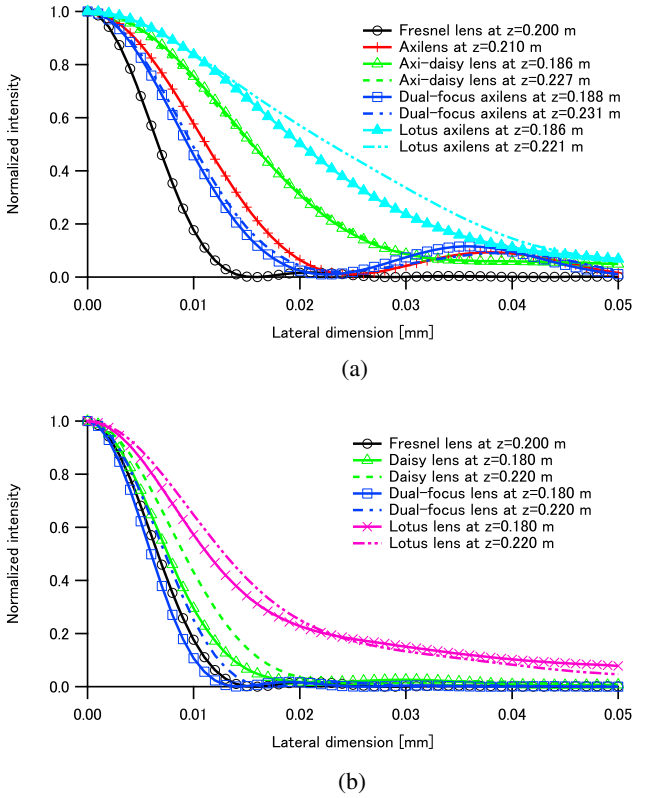

Fig. 5. (Color online) Normalized lateral intensity profiles at azimuthal angle of $\theta = 0$. (a) Fresnel lens (solid line marked with circle) and lens with long focus type, axi-daisy lens (solid line marked with open trangle and broken line), dual-focus axilens (solid line marked with square and chain line), and lotus axilens (solid line marked with filled triangle and two-dot chain line). (b) Fresnel lens (solid line marked with circle) and lens with dual focus type, daisy lens (solid line marked with trangle and broken line), dual-focus lens (solid line marked with square and chain line), and lotus lens (solid line marked with cross mark and two-dot chain line).

3.4 Petal dependency of diffraction intensity profile

The daisy lens, dual-focus lens, and lotus lens have circularly oscillated phase undulation. Those undulations look like the petals of a flower. We verified how the number of petals influences the focal intensity. Figure 7 shows the axial intensity profiles of two axi-daisy lenses with the numbers of petals $n = 3$ and 10. As shown in this figure, these are almost the same. We find that the number of lens petals does not influence the intensity distribution along the optical axis. The other types of lens showed a similar tendency.

Moreover, we examined the petal dependency on the focal spot shape. Figure 8 shows focal spots near the optical axis of two axi-daisy lenses with $n = 3$ and 10. It shows that the number of petals influences the intensity profile of the main spot. The central spot strongly reflects the polygonal shape of the object lens, when the number of petals is small. With increasing the number of petals, the spot becomes round.

4. Conclusions

We proposed some novel types of diffractive lens with dual and extended depth of focus, and numerically investigated their intensity profiles around the focal region. The new type of lens obtained the dual focus characteristic by radial groove undulation of the phase profile. Furthermore, combining those lenses with the axilens, they also received the long focus property simultaneously.

The daisy lens, dual-focus lens, and lotus lens have two separate intensity peaks (dual focus) along the optical axis. We can control the focus separation by the modulation depth of the phase undulation. The dual-focus lens has the smallest spot among them, which is comparable to the spot size of the Fresnel lens. The axi-daisy lens, dual-focus axilens, and lotus axilens, which are combined with the axilens, not only have the dual focus nature, but also extended depth of each

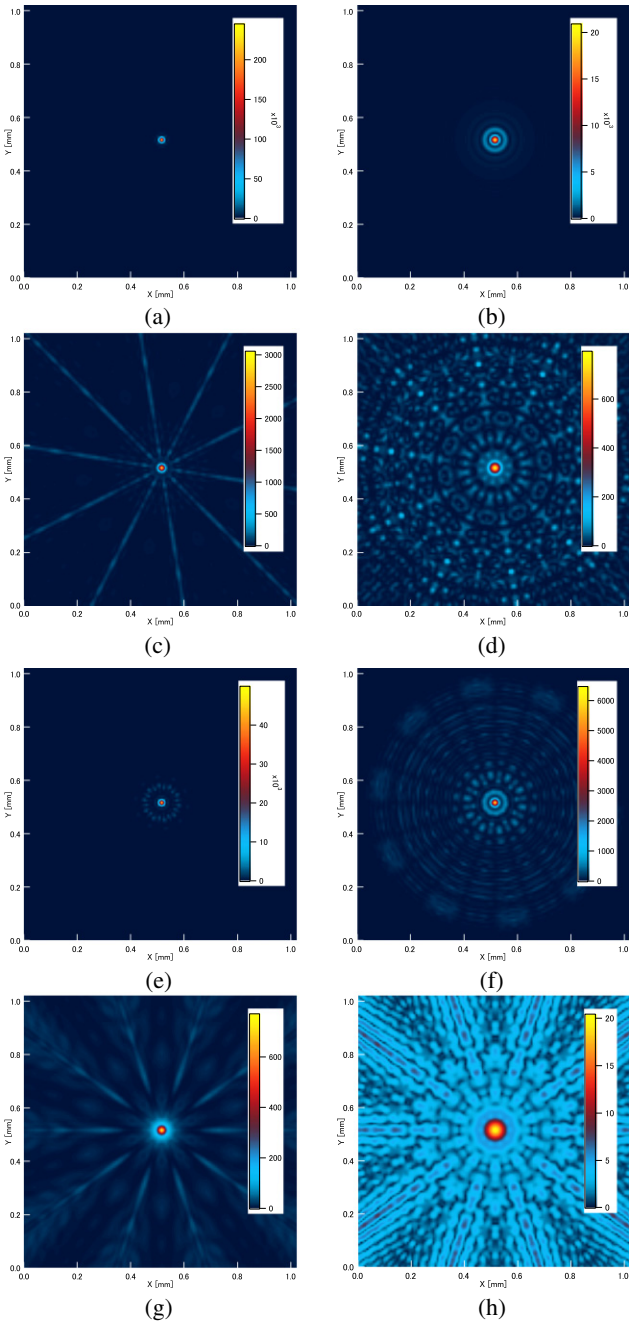

Fig. 6. (Color online) Diffraction patterns near the optical axis. (a) Fresnel lens at $z = 0.200$ m. (b) Axilens at $z = 0.209$ m. (c) Daisy lens at $z = 0.220$ m. (d) Axi-daisy lens at $z = 0.227$ m. (e) Dual-focus lens at $z = 0.220$ m. (f) Dual-focus axilens at $z = 0.231$ m. (g) Lotus lens at $z = 0.220$ m. (h) Lotus axilens at $z = 0.221$ m.

focus. The dual-focus axilens has the broadest axial intensity profile of all other lenses and keeps a long focal depth with a sharp focal spot. The lotus lens has only a weak dual focal spot, while it may have a comparatively long focal depth without combining the axilens. The lotus axilens has semi-periodic intensity distribution along the optical axis.

We also investigated how the number of lens petals influences the intensity distribution in the focal region. We found that the number of lens petals did not influence the axial intensity, but changed the spot shape of the diffraction pattern.

We did not intend that the simulation in this study would target specific discs such as DVDs and Blu-ray discs. We did not consider the reflection and refraction at the boundary of layers that exist in the disc media. The simulation including the Fresnel reflection and refraction at the interfaces among the layers is our future work. We expect that these diffractive lenses can be used in pickup systems by combining with other objectives to obtain the required spot size and focal length.

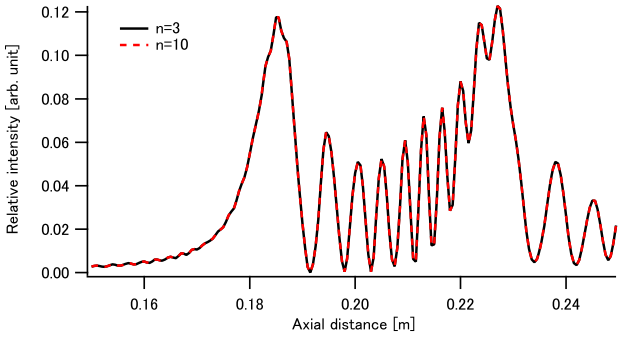

Fig. 7. (Color online) Axial intensity of three- and ten-petal axi-daisy lenses.

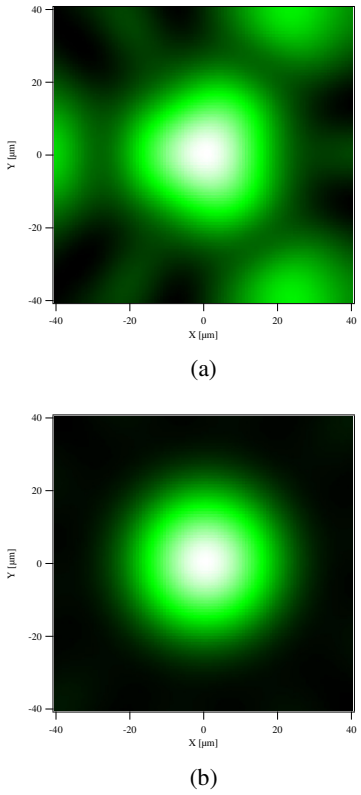

Fig. 8. (Color online) Focal spot images near the optical axis of axi-daisy lenses, for which the numbers of petals are (a) $n = 3$ and (b) $n = 10$.

References

1) N. Takahashi, H. Sato, H. Osawa, K. Nagai, H. Isobe, and I. Kasuga: Jpn. J. Appl. Phys. **36** (1997) 467.
2) Y. Komma, Y. Tanaka, K. Urairi, S. Nishino, and S. Mizuno: Jpn. J. Appl. Phys. **36** (1997) 474.
3) Y. Tsuchiya, S. Kajiyama, Y. Kano, Y. Matsumura, and S. Ichiura: Jpn. J. Appl. Phys. **36** (1997) 481.
4) C. W. Lee, C. S. Chung, K. H. Cho, P. Y. Seong, T.-K. Kim, S. Y. Jung, B. H. Choi, J. H. Yoo, J. E. Seo, and D. H. Shin: Jpn. J. Appl. Phys. **36** (1997) 486.
5) N. Davidson, A. A. Friesem, and E. Hasman: Opt. Lett. **16** (1991) 523.
6) J. H. McLeod: J. Opt. Soc. Am. **44** (1954) 592.
7) D. A. Buralli, G. M. Morris, and J. R. Rogers: Appl. Opt. **28** (1989) 976.
8) D. W. Sweeney and G. E. Sommargren: Appl. Opt. **34** (1995) 2469.
9) W. Daschner, B. Block, A. Thornton, and B. Kress: U.S. Patent 6330118B1 (2001).
10) M. Born and E. Wolf: *Principles of Optics* (Cambridge University Press, Cambridge, U.K., 1999) 7th ed., p. 423.
11) K. Matsushima: Opt. Express **18** (2010) 18453.
12) J. W. Goodman: *Introduction to Fourier Optics* (McGraw-Hill, New York, 1996) 2nd ed., p. 77.